Protein Engineering, Design & Selection vol. 24 no. 1–2 pp. 69–78, 2011
Published online November 12, 2010 doi:10.1093/protein/gzq100

Deletion of a Ure2 C-terminal prion-inhibiting region promotes the rate of fibril seed formation and alters interaction with Hsp40

Li Chen[1,2,†], Li-Jun Chen[1,†], Hai-Yan Wang[1,2], Yi-Qian Wang[1,2] and Sarah Perrett[1,*]

[1]National Laboratory of Biomacromolecules, Institute of Biophysics, Chinese Academy of Sciences, 15 Datun Road, Chaoyang District, Beijing 100101, China and [2]Graduate University of Chinese Academy of Sciences, 19 Yuquan Road, Shijingshan District, Beijing 100049, China

[*]To whom correspondence should be addressed.
E-mail: sarah.perrett@cantab.net

Received October 10, 2010; revised October 10, 2010; accepted October 12, 2010

Edited by Daniel Otzen

Prions are proteins that can undergo a heritable conformational change to an aggregated amyloid-like state, which is then transmitted to other similar molecules. Ure2, the nitrogen metabolism regulation factor of *Saccharomyces cerevisiae*, shows prion properties *in vivo* and forms amyloid fibrils *in vitro*. Ure2 consists of an N-terminal prion-inducing domain and a C-terminal functional domain. Previous studies have shown that mutations affecting the prion properties of Ure2 are not restricted to the N-terminal prion domain: the deletion of residues 151–158 in the C-domain increases the *in vivo* prion-inducing propensity of Ure2. Here, we characterized this mutant *in vitro* and found that the 151–158 deletion has minimal effect on the thermodynamic stability or folding properties of the protein. However, deletion of residues 151–158 accelerates the nucleation, growth and fragmentation of amyloid-like aggregates *in vitro*, and the aggregates formed are able to seed formation of fibrils of the wild-type protein. In addition, the absence of 151–158 was found to disrupt the inhibitory effect of the Hsp40 chaperone Ydj1 on Ure2 fibril formation. These results suggest that the enhanced *in vivo* prion-inducing ability of the 151–158 deletion mutant is due to its enhanced ability to generate prion seeds.

Keywords: amyloid/folding/prion/Ure2p/[*URE3*]

Introduction

Ure2 is the protein determinant of the [*URE3*] prion state in *Saccharomyces cerevisiae*. Analogous to the properties of the mammalian prion protein, Ure2 shows the ability to convey a heritable phenotype change by undergoing a structural change at the protein level to an amyloid-like form (Wickner, 1994; Masison and Wickner, 1995; Lian *et al.*, 2006; Perrett and Jones, 2008). Ure2 functions as a nitrogen metabolism regulation factor in *Saccharomyces cerevisiae* by interacting with the transcription factor Gln3, allowing control of nitrogen catabolite repression and blocking the uptake of poor nitrogen sources in the presence of a good nitrogen source (Coschigano and Magasanik, 1991; Cooper, 2002); this function is inactivated upon transformation of Ure2 to the prion state. Ure2 is a 354-amino acid homodimeric protein consisting of a relatively flexible N-terminal domain and a globular C-terminal domain (Perrett *et al.*, 1999; Thual *et al.*, 1999; Bousset *et al.*, 2001a; Umland *et al.*, 2001). The unstructured N-terminal domain (~90 amino acids) is required for both the prion properties *in vivo* (Masison and Wickner, 1995) and amyloid formation *in vitro* (Taylor *et al.*, 1999; Thual *et al.*, 2001; Jiang *et al.*, 2004), and is thus referred to as the prion-inducing domain (PrD). The C-terminal domain shows structural similarity to the glutathione *S*-transferase superfamily (Bousset *et al.*, 2001a; Umland *et al.*, 2001) and is both necessary and sufficient for its *in vivo* nitrogen regulatory function (Coschigano and Magasanik, 1991; Cooper, 2002). The C-terminal domain of Ure2 binds glutathione (GSH) (Bousset *et al.*, 2001b) and shows GSH-dependent peroxidase (GPx) (Bai *et al.*, 2004) and glutaredoxin (GRX) activities (Zhang and Perrett, 2009).

Protein sequence analysis of Ure2 has demonstrated that the PrD is generally divergent and rich in Asn and Gln residues, but contains a relatively conserved region, corresponding to residues 10–40, which contains normal random sequence (Edskes and Wickner, 2002). Studies have shown that deletions of Asn/Gln repeats in the PrD reduce the prion inducing ability *in vivo* and the amyloid formation *in vitro* of Ure2 (Maddelein and Wickner, 1999; Jiang *et al.*, 2004); deletion of the normal random sequence (residues 15–42) also results in decreased fibril formation of Ure2 *in vitro* (Jiang *et al.*, 2004). In contrast to the importance of the PrD in the prion induction and amyloid formation of Ure2, the deletion of the PrD has no detectable effect on the dimeric structure, thermodynamic stability and folding kinetics of Ure2 under a wide range of conditions (Perrett *et al.*, 1999; Thual *et al.*, 2001; Zhou *et al.*, 2001; Galani *et al.*, 2002; Zhu *et al.*, 2003a,b). Amyloid-like fibrils of Ure2 are thought to form by conversion of the PrD to a parallel in-register β-sheet structure (Baxa *et al.*, 2005, 2007) surrounded by the C-terminal domains in a native-like conformation, which is suggested by both our previous studies in which Ure2 maintains native-like activity in the fibrillar form (Bai *et al.*, 2004; Zhang *et al.*, 2008; Zhang and Perrett, 2009) and other studies in which heterologous proteins fused to the PrD retain their enzymatic activity in amyloid fibrils (Baxa *et al.*, 2002). Therefore, the loss of regulatory function of Ure2 associated with prion formation is likely to be due to a steric effect rather than the loss of native structure.

However, previous studies have suggested the involvement of the C-terminal region of Ure2 in its prion properties, suggesting interplay between the roles of the PrD and the

[†]These authors contributed equally to this work.

C-terminal region. A number of deletions in the C-terminal region have been found to increase or decrease the *in vivo* prion-inducing propensity of Ure2 when overexpressed in a wild-type (WT) background: deletion of residues 221–227 decreases prion induction (Maddelein and Wickner, 1999), and the deletion of 151–158 or 348–354 increases the rate of prion induction (Masison and Wickner, 1995). Interestingly, while deletion of residues 1–65 removes prion inducing ability, the combined deletion of this and the regions 151–158 and 348–354 produces a fragment that can once again induce prion formation (Maddelein and Wickner, 1999). Studies on the structural and folding properties of these mutants may yield important insight into the molecular mechanism of prion induction and propagation.

A key feature of prion disease is protein misfolding leading to formation of amyloid-like aggregates. Studying the relationship between protein folding and amyloid formation is a prerequisite to elucidating the molecular mechanism of prion formation. In this study, we constructed a C-terminal mutant of Ure2 lacking residues 151–158, which we term Δ151–158 Ure2, as well as further mutants with additional deletions within the PrD (Fig. 1). We then characterized the equilibrium denaturation and amyloid formation of these mutants, with the purpose of elucidating the mechanism by which the deletion of the C-terminal residues 151–158 increases the *in vivo* prion inducing ability of Ure2 and thus providing insight into the relationship between the molecular mechanism of prion formation of Ure2 and its folding properties.

Materials and methods

Materials

GdmCl, Tris and ThT were obtained from Sigma. Other chemical regents were local products of analytical grade. Twice deionized water was used throughout. Solutions were made volumetrically. Concentrations of GdmCl solutions were confirmed by use of an Abbe refractometer.

Mutant construction and protein purification

All mutants of Ure2 were obtained by PCR using a synthetic WT URE2 gene as a template (Perrett *et al.*, 1999) and confirmed by DNA sequencing of the entire gene. Ure2 and mutants were expressed in *Escherichia coli* and purified as described previously (Perrett *et al.*, 1999) except that a French press was used to lyse cells in place of sonication. Proteins were stored at −80°C and defrosted in a 25°C water bath immediately prior to use. Samples were prepared in 50 mM Tris–HCl buffer, pH 8.4 containing 0.2 M NaCl unless stated otherwise and centrifuged at 18 000 *g* for 30 min at 4°C to remove any aggregated protein before experiments. The protein concentration in terms of monomers was measured by absorbance at 280 nm using the calculated extinction coefficient of 48 200 M^{-1} cm^{-1} (Perrett *et al.*, 1999). Ydj1 was purified as described previously (Lian *et al.*, 2007).

Equilibrium denaturation measurements

The equilibrium denaturation of Ure2 or mutants was investigated by following the changes in intrinsic tryptophan fluorescence as described previously (Zhu *et al.*, 2003b). Δ15–42 Ure2 was used as a pseudo WT, due to its enhanced solubility and reversibility of folding, as described previously (Perrett *et al.*, 1999; Galani *et al.*, 2002; Zhu *et al.*, 2003b). Data analysis and curve fitting were performed as described (Zhu *et al.*, 2003b). The methods for fluorescence measurements and data analysis are briefly outlined below.

Sample preparation. Equilibrium denaturation curves were measured in 50 mM Tris–HCl buffer, pH 8.4, containing 0.2 M NaCl, conditions found to provide optimum solubility and reversibility of folding, particularly for the full-length Ure2 or Δ15–42 Ure2 (Perrett *et al.*, 1999). GdmCl was chosen as the denaturant and 8 M GdmCl was prepared in the same buffer. Samples denatured in different concentrations of GdmCl were prepared and allowed to equilibrate overnight at 25°C before taking measurements.

Intrinsic fluorescence measurements. All measurements were performed at 25°C using a Hitachi F-4500 or Shimadzu RF-5301PC spectrofluorimeter. Excitation was at 280 nm and emission spectra were measured between 300 and 400 nm. The maximum change in fluorescence intensity upon denaturation was observed at 327 nm and under

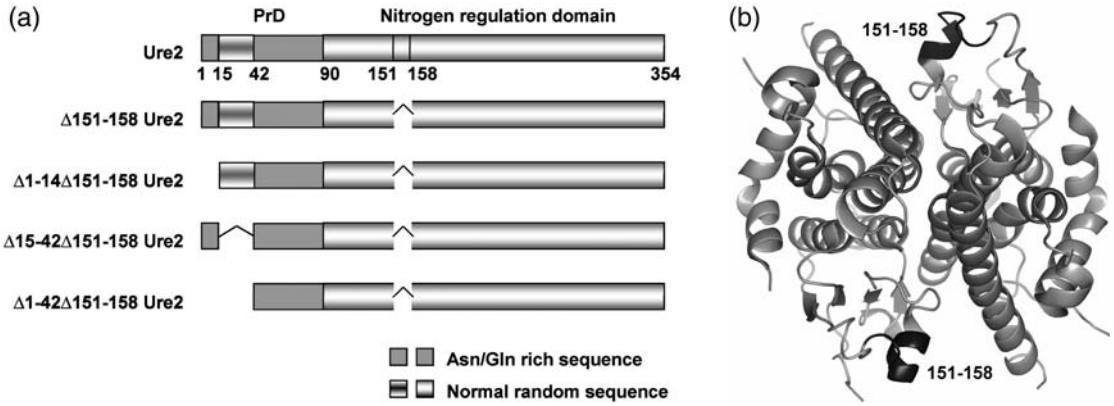

Fig. 1. Structure of Ure2 and its mutants. (**a**) Schematic diagram showing the primary structure of Ure2 mutants used in the study. (**b**) Ribbon diagram showing the location of residues 151–158 in the Ure2 structure. The figure was produced with the PyMOL Molecular Graphics System (Schrödinger, LLC), using pdb file 1G6W (Bousset *et al.*, 2001a).

apparent two-state conditions, an isosbestic point at 369 nm was observed (Perrett *et al.*, 1999). The denaturation curves were made by plotting the ratios of fluorescence intensity at 327 nm to that of 369 nm versus [GdmCl] after normalization. The final concentration of the protein in terms of monomer in the denaturation samples ranged from 0.5 to 5 μM.

Data analysis of the equilibrium unfolding. The equilibrium denaturation curves were fitted to the model of three-state unfolding via a homodimeric intermediate ($N_2 \Leftrightarrow I_2 \Leftrightarrow 2U$) as described in detail previously (Zhu *et al.*, 2003b). The model is briefly outlined below. It was shown previously from detailed study over a range of protein concentrations and other experimental conditions that even where the denaturation transition appears two-state for Ure2, a more accurate estimate of the thermodynamic stability is obtained for this protein by fitting the apparent two-state transition to a three-state model (Zhu *et al.*, 2003b). This is achievable because the amplitude of the fluorescence signal for the intermediate state is routinely used as a fixed parameter (see below). Non-linear least-squares fitting of the data was carried out using the regression wizard of the SigmaPlot software.

The amplitude of the spectroscopic signal determined at each denaturant concentration is assumed to be a linear combination of the fractional contribution from each species:

$$y = f_N(y_N + m_N[\text{GdmCl}]) + f_I y_I + f_U(y_U + m_U[\text{GdmCl}]) \quad (1)$$

where y_N, y_U, m_N and m_U are the intercepts and slopes of the initial and final baselines, respectively; y_I is the amplitude of the signal for the intermediate state, which is assumed not to vary with [GdmCl] in order to minimize the number of parameters in the fit (Grimsley *et al.*, 1997) and f_N, f_I and f_U are the fraction of native, intermediate and denatured states, respectively.

The equilibrium constants for the two transitions are given by $K_1 = [I_2]/[N_2]$ and $K_2 = [U]^2/[I_2]$. The total protein concentration expressed as monomer is $C = 2[N_2] + 2[I_2] + [U]$ and $f_N + f_I + f_U = 1$. Hence $f_N = 2[N_2]/C$; $f_I = 2[I_2]/C$ and $f_U = [U]/C$. From these relationships, f_N, f_I and f_U can be solved and expressed using K_1, K_2 and C as shown below:

$$f_U = \frac{-K_1K_2 + \sqrt{(K_1K_2)^2 + 8C(1+K_1)K_1K_2}}{4C(1+K_1)}$$
$$f_I = \frac{2Cf_U^2}{K_2}$$
$$f_N = 1 - f_I - f_U \quad (2)$$

The free energy for unfolding, $\Delta G_U = -RT\ln K$, shows a linear relationship with the denaturant concentration (Tanford, 1968)

$$\Delta G_U = \Delta G_U(H_2O) - m[\text{GdmCl}] \quad (3)$$

where m is the denaturant dependence (or slope) of the transition and $\Delta G_U(H_2O)$ is the free energy of unfolding in the absence of denaturant. Assuming the two transitions are distinct, the midpoint of the first transition occurs when $f_N = f_I$ and so $K_1 = 1$, hence:

$$\Delta G_1(H_2O) = m_1[\text{GdmCl}]_{1/2,1} \quad (4)$$

$$K_1 = \exp\left(\frac{m_1([\text{GdmCl}] - [\text{GdmCl}]_{1/2,1})}{RT}\right) \quad (5)$$

Similarly, the midpoint of the second transition occurs when $f_I = f_U = 1/2$ and so $K_2 = C$; hence:

$$\Delta G_2(H_2O) = m_2[\text{GdmCl}]_{1/2,2} - RT\ln C \quad (6)$$

$$K_2 = \exp\left(\frac{m_2([\text{GdmCl}] - [\text{GdmCl}]_{1/2,2})}{RT} + \ln C\right) \quad (7)$$

where m_1 and m_2 are the slopes, and $[\text{GdmCl}]_{1/2,1}$ and $[\text{GdmCl}]_{1/2,2}$ are the midpoints of the first and second transitions, respectively. The values of m_1, m_2, $[\text{GdmCl}]_{1/2,1}$ and $[\text{GdmCl}]_{1/2,2}$ are obtained by fitting the data to equation (1), having substituted for f_N, f_I and f_U in terms of m_1, m_2, $[\text{GdmCl}]_{1/2,1}$ and $[\text{GdmCl}]_{1/2,2}$ using the expressions given in equations (2), (5) and (7). Thus, the free energy change of the first and second transition can be obtained from equations (4) and (6), respectively, and the overall stability of the protein according to this model is obtained from:

$$\Delta G_U(H_2O) = \Delta G_1(H_2O) + \Delta G_2(H_2O) \quad (8)$$

ThT binding assay

The kinetics of amyloid formation of Ure2 and mutants was monitored using the ThT binding assay as described previously (Zhu *et al.*, 2003b; Jiang *et al.*, 2004). Briefly, a volume of 300 μl Ure2 or its mutant was pipetted into a 2 ml microcentrifuge tube and a 3 mm diameter glass sphere (Fisher) was added. NaN_3 (0.02% w/v) was added to prevent bacterial growth. The tubes were incubated at 37°C or 25°C, as indicated, with agitation at 200 rpm. Alternatively, proteins were incubated at 4°C without agitation. At regular time intervals, 10 μl aliquots were removed from the incubated mixture and assayed for ThT binding. For each sample, the intensity of ThT fluorescence at 485 nm excited by 450 nm was measured on a Hitachi F-4500 or Shimadzu RF-5301PC spectrofluorimeter. Samples were incubated in parallel whenever possible.

EM imaging

The morphology of fibrils was confirmed by electron microscopy (EM). A 10 μl aliquot of protein was adsorbed onto a glow-discharged carbon support film for 1 min and washed twice with 10 μl distilled water. Excess solution was blotted off with a filter paper. Specimens were negatively stained with uranyl acetate (2%, w/v) and examined on a Philips Tecnai 20 electron microscope. Images were collected by CCD camera.

Cross-seeding experiments

Seed preparation. WT Ure2 or Δ151–158 Ure2 was incubated at a concentration of 40 μM at 4°C in 50 mM

Tris–HCl, pH 8.4, 200 mM NaCl for at least 10 days, by which time polymerization was complete as measured by ThT assay. Mature fibrils were then sonicated using a probe sonicator (Sonics and Materials VCX750) for 5 s (22% energy) in order to produce the seeds used in the solution seeding experiments.

Cross-seeding. Twenty micromolar WT Ure2 or Δ151–158 Ure2 protein was incubated with a series of concentrations (0, 1, 2, 4, 7 and 10%) of pre-prepared WT Ure2 or Δ151–158 Ure2 seeds at 4°C without agitation in 50 mM Tris–HCl, pH 8.4, 200 mM NaCl. The kinetics of fibril formation was monitored by the ThT assay as described above.

Data analysis. The ThT fluorescence values at intermediate times were converted into concentrations of protein in fibrillar form by using a linear scaling between the initial and final fluorescence values (Y.Q.W., A. Buell, X.Y. Wang, M. Welland, C.M. Dobson, T.P.J. Knowles and S.P., submitted for publication). The kinetic data for fibril formation were then fitted globally to an explicit analytical solution to the master equation of fibrillar growth derived previously which has a double exponential form (Knowles *et al.*, 2009):

$$\frac{M(t)}{m_0} = 1 - \exp(-C_1 e^{\kappa t} + C_2 e^{-\kappa t}) \tag{9}$$

where the constants are fixed by the initial conditions:

$$C_{1,2} = \frac{k_+ P_0}{\kappa} \pm \frac{F_0}{2m_0} \tag{10}$$

where P_0 is the number and $F_0 = P_0 L_0$ the mass concentration of seed fibrils at $t = 0$, which are related through L_0, the average number of molecular units in a seed fibril; m_0 is the initial concentration of soluble Ure2p; and k_+ is the rate constant for fibril elongation. The single effective rate constant κ describes the rate of growth of the fibril population through the concerted action of fragmentation and elongation:

$$\kappa = \sqrt{2 m_0 k_+ k_-} \tag{11}$$

where k_- is the rate constant for fragmentation. This allows two free global parameters to be determined, defined as $\xi_1 = k_+/L_0$ and $\xi_2 = k_+ k_-$, which can be obtained through fitting the kinetics of fibril formation. In order to remove the issue of comparing different batches of protein seeds, and also to circumvent the difficulty of defining the actual value of L_0, cross-seeding was used and comparison was carried out using ratios of the rate constants (Y.Q.W., A. Buell, X.Y. Wang, M. Welland, C.M. Dobson, T.P.J. Knowles, and S.P., submitted for publication). This means that L_0 is constant within a given cross-seeding experiment and the L_0 term cancels out. The ratios of the elongation rates (r_+) or breakage rates (r_-) for mutant and WT Ure2 were then calculated for both types of seeds as follows:

$$r_+^{\mathrm{WT}} = \frac{k_+^{\mathrm{WT}|\Delta 151-158}}{k_+^{\mathrm{WT}|\mathrm{WT}}} = \frac{\xi_1^{\mathrm{WT}|\Delta 151-158}}{\xi_1^{\mathrm{WT}|\mathrm{WT}}} \tag{12}$$

$$r_+^{\Delta 151-158} = \frac{k_+^{\Delta 151-158|\Delta 151-158}}{k_+^{\Delta 151-158|\mathrm{WT}}} = \frac{\xi_1^{\Delta 151-158|\Delta 151-158}}{\xi_1^{\Delta 151-158|\mathrm{WT}}} \tag{13}$$

$$r_-^{\mathrm{WT}} = \frac{k_-^{\mathrm{WT}|\Delta 151-158}}{k_-^{\mathrm{WT}|\mathrm{WT}}} = \frac{\xi_1^{\mathrm{WT}|\mathrm{WT}}\,\xi_2^{\mathrm{WT}|\Delta 151-158}}{\xi_1^{\mathrm{WT}|\Delta 151-158}\,\xi_2^{\mathrm{WT}|\mathrm{WT}}} \tag{14}$$

$$r_-^{\Delta 151-158} = \frac{k_-^{\Delta 151-158|\Delta 151-158}}{k_-^{\Delta 151-158|\mathrm{WT}}} = \frac{\xi_1^{\Delta 151-158|\mathrm{WT}}\,\xi_2^{\Delta 151-158|\Delta 151-158}}{\xi_1^{\Delta 151-158|\Delta 151-158}\,\xi_2^{\Delta 151-158|\mathrm{WT}}} \tag{15}$$

where $r_\pm^{\mathrm{WT}}$ and $r_\pm^{\Delta 151-158}$ denote seeding with WT and Δ151–158 Ure2, respectively; $k_\pm^{\mathrm{WT}|\Delta 151-158}$ denotes rate constants measured for soluble Δ151–158 Ure2 protein when seeded by fibrils formed from WT Ure2; $k_\pm^{\Delta 151-158|\mathrm{WT}}$ denotes rate constants measured for soluble WT Ure2 protein when seeded by fibrils formed from Δ151–158 Ure2; and $k_\pm^{\mathrm{WT}|\mathrm{WT}}$ and $k_\pm^{\Delta 151-158|\Delta 151-158}$ denote self-seeded samples for WT and Δ151–158 Ure2, respectively. A value of $r_\pm = 1$ for a given type of seed indicates that the nature of the soluble protein does not influence the rate constants, whereas $r_\pm > 1$ for a given type of seed indicates that fibrils formed from the mutant protein elongate or fracture faster than WT fibrils.

In order to compare the effects associated with the nature of the seed, we introduce the ratio:

$$\eta_\pm = \frac{r_\pm^{\Delta 151-158}}{r_\pm^{\mathrm{WT}}} \tag{16}$$

A value of $\eta_\pm = 1$ indicates that the nature of the seed does not affect the rate constants for elongation (+) or breakage (−).

Results and discussion

Deletion of residues 151–158 does not affect the secondary structure of Ure2

As shown in Fig. 2, WT Ure2 and Δ151–158 Ure2 showed very similar far-UV CD spectra, indicating that the deletion of residues 151–158 does not substantially disrupt the overall helical secondary structural content of Ure2.

The deletion of residues 151–158 does not alter the thermodynamic stability of the protein

As mentioned above, understanding the stability and folding properties of prion proteins is a prerequisite to elucidate the molecular mechanism of prion formation. Identification and characterization of folding intermediates is a crucial step in evaluating plausible mechanisms for prion conversion and propagation. The folding properties of Ure2 have been studied in detail (Perrett *et al.*, 1999; Thual *et al.*, 2001; Galani *et al.*, 2002; Zhu *et al.*, 2003a,b). Equilibrium denaturation indicates that Ure2 undergoes a three-state unfolding process via a dimeric intermediate (Zhu *et al.*, 2003b). Here,

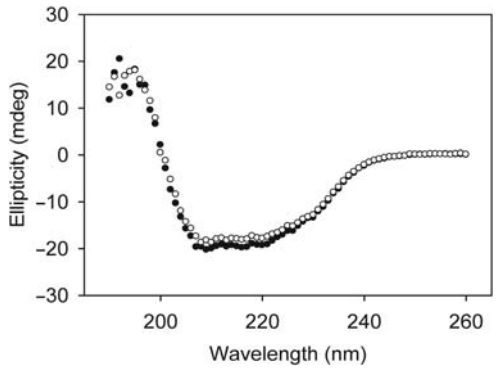

Fig. 2. CD spectra of WT and Δ151–158 Ure2. Spectra were measured in the far-UV region (190–260 nm) for 40 μM WT Ure2 (closed circle) and Δ151–158 Ure2 (open circle) in 50 mM Tris–HCl, pH 8.4, 200 mM NaCl at 25°C.

we examined the effect of the deletion of residues 151–158 on the stability of Ure2. We made use of a variant of Ure2, Δ15–42 Ure2 as a pseudo WT, due to its exceptional solubility and identical folding behavior to WT Ure2 (Perrett *et al.*, 1999; Galani *et al.*, 2002; Zhu *et al.*, 2003b). A direct role of residues 15–42 in amyloid formation has been proposed and would explain the increased solubility of the Δ15–42 Ure2 protein (Jiang *et al.*, 2004).

Similar to Δ15–42 Ure2, the equilibrium denaturation of Δ151–158 Ure2 showed a three-state unfolding transition (Fig. 3a). The unfolding profile of Δ151–158 Ure2 involved two transitions: the first transition did not show dependence on the protein concentration and corresponds to partial unfolding of the protein, while the second transition showed protein concentration dependence and corresponds to the dissociation and unfolding of the dimeric intermediate (Fig. 3a), as found previously for the WT protein and its N-terminal deletion mutants (Zhu *et al.*, 2003b). The thermodynamic parameters were obtained by fitting the denaturation curves of Δ151–158 Ure2 at different concentrations to a three-state model (see Materials and Methods section and Table I). Compared with Δ15–42 Ure2, Δ151–158 Ure2 showed lower midpoints for both transitions, $[GdmCl]_{1/2,1}$ and $[GdmCl]_{1/2,2}$ (Fig. 3b and Table I). However, this was accompanied by a greater slope (*m*-value), particularly for the first transition, with the result that the calculated apparent free energy changes for the two individual transitions, $\Delta G_1(H_2O)$ and $\Delta G_2(H_2O)$, and for the overall unfolding process, $\Delta G_U(H_2O)$, are the same within error for the pseudo WT and for the Δ151–158 mutant (Table I).

The effect of the PrD on the stability of Δ151–158 Ure2 was also examined. As was found previously for the WT protein (Perrett *et al.*, 1999; Thual *et al.*, 2001; Galani *et al.*, 2002; Zhu *et al.*, 2003a,b), deletion of parts of the PrD (to produce the double-deletion mutants Δ1–14Δ151–158 Ure2, Δ15–42Δ151–158 Ure2 or Δ1–42Δ151–158 Ure2, Fig. 1a) had no effect on the stability or folding behavior of the protein (Fig. 3c and Table I).

Taken together, these results indicate that the deletion of residues 151–158 has no effect on the stability of the Ure2 protein or its equilibrium denaturation behavior, suggesting that the altered prion-inducing propensity observed for the Δ151–158 mutant *in vivo* (Masison and Wickner, 1995; Maddelein and Wickner, 1999) is unlikely to be due to altered folding of the C-domain of the Ure2 protein.

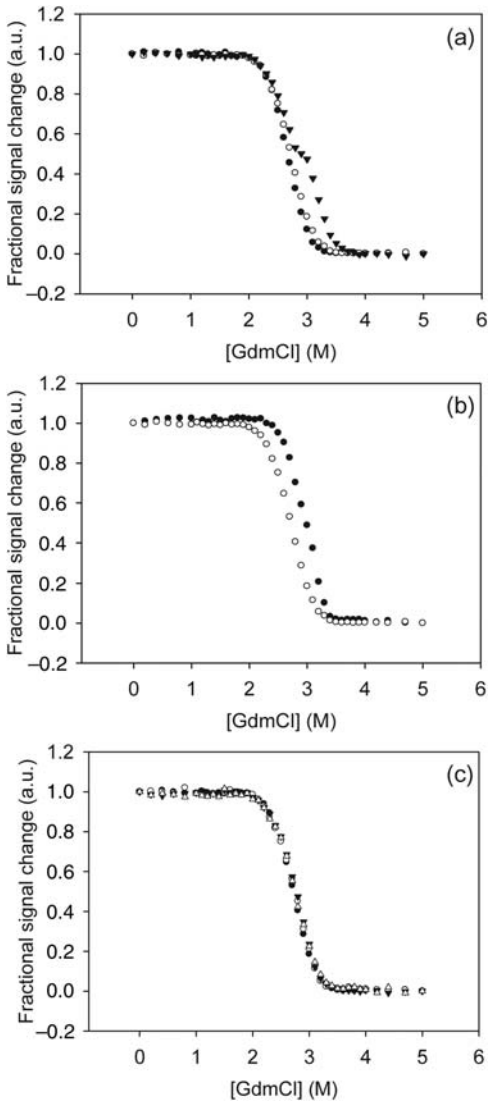

Fig. 3. Equilibrium denaturation of Δ151–158 Ure2. (**a**) Effect of protein concentration. Data are shown for 0.5 μM (closed circle), 1 μM (open circle) and 5 μM (closed inverted triangle) Δ151–158 Ure2 in 50 mM Tris–HCl, pH 8.4, with 200 mM NaCl at 25°C. (**b**) Comparison of Δ151–158 Ure2 with Δ15–42 Ure2 (pseudo WT). Data are shown for 1 μM Δ15–42 Ure2 (closed circle) and Δ151–158 Ure2 (open circle) in 50 mM Tris–HCl, pH 8.4, with 200 mM NaCl at 25°C. (**c**) Effect of deletions in the PrD. Data are shown for 1 μM Δ151–158 Ure2 (closed circle), Δ1–14Δ151–158 Ure2 (open circle), Δ15–42Δ151–158 Ure2 (closed inverted triangle) and Δ1–42Δ151–158 Ure2 (open triangle) in 50 mM Tris–HCl, pH 8.4, with 200 mM NaCl, at 25°C.

Deletion of residues 151–158 accelerates the rate of amyloid-like aggregation of Ure2 while deletions in the PrD modulate the kinetics and morphology of aggregation

Fibrils formed *in vitro* bind ThT, a dye considered highly specific for amyloid, and emit specific fluorescence at 485 nm. Thus, ThT binding provides a convenient method to assay the kinetics of amyloid formation (LeVine, 1993). Previous studies have demonstrated that the time course of Ure2 amyloid formation monitored by ThT binding shows a sigmoidal curve, representing a lag time corresponding to a nucleation process, an exponential elongation phase and a

Table I. Thermodynamic stability of Δ15–42 Ure2 (pseudo WT) and Δ151–158 Ure2 mutants[a]

Protein	[Protein] (μM)	$[GdmCl]_{1/2,1}$ (M)	$[GdmCl]_{1/2,2}$ (M)	m_1 (kJ $mol^{-1}M^{-1}$)	m_2 (kJ $mol^{-1}M^{-1}$)	ΔG_1 (H_2O) (kJ mol^{-1})	$\Delta G_2(H_2O)$ (kJ mol^{-1})	$\Delta G_U(H_2O)$ (kJ mol^{-1})
Δ15–42 Ure2[b] (pseudo WT)	0.5	2.78 ± 0.02	3.11 ± 0.01	16.4 ± 0.7	36 ± 3	47 ± 2	147 ± 10	194 ± 11
	1	2.80 ± 0.01	3.22 ± 0.01	18.0 ± 0.7	36 ± 1	50 ± 2	150 ± 2	200 ± 4
	5	2.77 ± 0.01	3.35 ± 0.01	18.1 ± 0.5	40 ± 2	50 ± 2	165 ± 6	215 ± 7
	Mean	2.78 ± 0.01	3.22 ± 0.01[c]	17.5 ± 0.6	37 ± 2	49 ± 1	154 ± 6	203 ± 6
Δ151–158 Ure2	0.5	2.47 ± 0.02	2.97 ± 0.02	19.7 ± 0.2	32 ± 3	48.9 ± 0.7	136 ± 7	180 ± 7
	1	2.52 ± 0.02	2.95 ± 0.03	19.7 ± 0.2	36 ± 4	49.6 ± 0.5	140 ± 7	189 ± 11
	5	2.51 ± 0.02	3.12 ± 0.04	20.0 ± 0.1	43 ± 6	50.4 ± 0.2	162 ± 11	215 ± 15
	Mean	2.50 ± 0.01	2.95 ± 0.03[c]	19.8 ± 0.1	37 ± 3	49.6 ± 0.4	145 ± 8	195 ± 9
Δ1–14Δ151–158 Ure2	0.5	2.47 ± 0.01	3.02 ± 0.01	19.8 ± 0.1	36 ± 2	49.0 ± 0.1	145 ± 4	194 ± 4
	1	2.50 ± 0.01	3.02 ± 0.01	19.9 ± 0.1	37 ± 1	49.8 ± 0.2	145 ± 2	195 ± 2
	5	2.51 ± 0.01	3.18 ± 0.01	19.9 ± 0.2	40 ± 1	49.9 ± 0.3	159 ± 2	209 ± 1
	Mean	2.49 ± 0.01	3.02 ± 0.01[c]	19.9 ± 0.1	37 ± 2	49.6 ± 0.3	150 ± 5	199 ± 5
Δ15–42Δ151–158 Ure2	0.5	2.49 ± 0.01	3.01 ± 0.01	19.8 ± 0.1	34 ± 2	49.3 ± 0.4	138 ± 4	187 ± 4
	1	2.53 ± 0.01	3.05 ± 0.01	20.0 ± 0.1	37 ± 1	50.6 ± 0.2	146 ± 3	196 ± 3
	5	2.52 ± 0.01	3.18 ± 0.01	20.0 ± 0.1	40 ± 3	50.3 ± 0.2	158 ± 8	208 ± 9
	Mean	2.51 ± 0.02	3.05 ± 0.01[c]	19.9 ± 0.1	37 ± 2	50.1 ± 0.4	147 ± 6	197 ± 6
Δ1–42Δ151–158 Ure2	0.5	2.48 ± 0.01	3.02 ± 0.01	19.9 ± 0.1	34 ± 1	49.4 ± 0.1	138 ± 2	188 ± 2
	1	2.50 ± 0.01	3.02 ± 0.01	20.0 ± 0. 1	38 ± 3	50.0 ± 0.2	149 ± 9	199 ± 9
	5	2.51 ± 0.01	3.20 ± 0.01	19.9 ± 0.1	42 ± 1	50.0 ± 0.3	164 ± 2	214 ± 2
	Mean	2.50 ± 0.01	3.02 ± 0.01[c]	19.9 ± 0.1	38 ± 3	49.8 ± 0.2	150 ± 8	200 ± 8
All Δ151–158 mutants	Mean	2.50 ± 0.01	3.01 ± 0.01[c]	19.9 ± 0.1	37 ± 1	49.8 ± 0.2	148 ± 3	198 ± 3

[a]Folding was monitored by intrinsic fluorescence in 50 mM Tris–HCl buffer, pH 8.4, with 200 mM NaCl at 25°C. Data were fitted to a three-state dimeric intermediate unfolding model (see Materials and Methods section). In each case, the error shown is the standard error of the mean of at least three experiments. $[GdmCl]_{1/2}$ is the midpoint and m is the slope of the transition; $\Delta G_1(H_2O) = m_1\,[GdmCl]_{1/2,1}$; $\Delta G_2(H_2O) = m_2\,[GdmCl]_{1/2,2} - RT \ln C$, where C is the total monomeric protein concentration; $\Delta G_U(H_2O) = \Delta G_1(H_2O) + \Delta G_2(H_2O)$ for the three-state model. Free energy values for dissociation/unfolding were shown for standard conditions, i.e. 1 M protein concentration.
[b]Data of Δ15–42 Ure2 could only be fitted to a three-state model by using a fixed value for y_I (of 0.43), in order to limit the number of fitting parameters, where y_I is the normalized spectroscopic intensity of the intermediate.
[c]The value for 1 μM protein concentration is shown.

plateau region (Schlumpberger *et al.*, 2000; Bousset *et al.*, 2002; Zhu *et al.*, 2003b). We have shown previously that for WT Ure2, the increase in ThT fluorescence correlates directly with the first appearance of fibrillar structures by atomic force microscopy (AFM) (Jiang *et al.*, 2004), and the ThT fluorescence signal is linearly proportional to the concentration of the Ure2 protein in fibrillar form (Y.Q.W., A. Buell, X.Y. Wang, M. Welland, C.M. Dobson, T.P.J. Knowles and S.P., submitted for publication). However, in the case of deletion mutants of Ure2, the degree of ThT fluorescence can be dramatically affected. In particular, deletion of the residues 15–42 was found to dramatically reduce the ability of Ure2 to bind ThT, although the ability to form fibrils was maintained (Jiang *et al.*, 2004). Therefore, ThT binding results are best interpreted in combination with fibril imaging techniques such as AFM or EM.

Here, we found that compared with WT Ure2, the time course of Δ151–158 Ure2 amyloid formation showed a similar sigmoidal curve but with a shorter lag time (Fig. 4). This suggests that the deletion of residues 151–158 enhances the ability of Ure2 to form amyloid fibrils *in vitro*, which is consistent with the *in vivo* result that this deletion increases its prion inducing ability (Maddelein and Wickner, 1999).

While Δ151–158 Ure2 showed a higher ThT fluorescence intensity in the plateau region than WT, the additional deletion of residues 1–14, 15–42 or 1–42 of the PrD (to produce the double-deletion mutants Δ1–14Δ151–158 Ure2, Δ15–42Δ151–158 Ure2 or Δ1–42Δ151–158 Ure2) dramatically lowered the fluorescence intensity in the plateau phase (Fig. 4). In the case of Δ1–14Δ151–158 Ure2, a sigmoidal shape to the curve was still detectible, allowing it to be seen

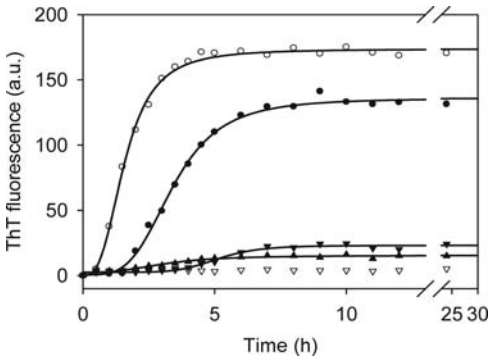

Fig. 4. Amyloid formation monitored by ThT binding. Data are shown for 30 μM WT Ure2 (closed circle), Δ151–158 Ure2 (open circle), Δ1–14Δ151–158 Ure2 (closed inverted triangle), Δ1–42Δ151–158 Ure2 (open inverted triangle) and Δ15–42Δ151–158 Ure2 (closed triangle). Incubation was in 50 mM Tris–HCl, pH 7.2 with 200 mM NaCl at 37°C with agitation.

that deletion of residues 1–14 results in a significant increase in the lag time (Fig. 4), as was also found previously for WT Ure2 (Jiang *et al.*, 2004). These results suggest that the PrD modulates the fibril formation of Δ151–158 Ure2 in a similar way as it does for WT.

However, unlike the typical fibril morphology of WT Ure2 fibrils (Fig. 5a), the morphology of fibrils formed from Δ151–158 Ure2 and Δ1–14Δ151–158 Ure2 observed by EM showed predominantly granular aggregates (Fig. 5b and c). These granular aggregates apparently also contain ordered structure because they could bind to the dye ThT and emit fluorescence (LeVine, 1993) (Fig. 4). Most interestingly, the further deletion of residues 15–42 restored the morphology

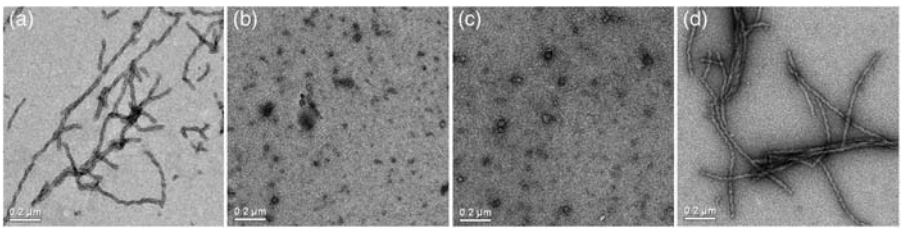

Fig. 5. EM images of fibrils in the plateau phase of fibril formation. (**a**) 40 μM WT Ure2, (**b**) 40 μM Δ151–158 Ure2, (**c**) 80 μM Δ1–14Δ151–158 Ure2 and (**d**) 80 μM Δ15–42Δ151–158 Ure2. Fibrils were incubated in 50 mM Tris–HCl, pH 8.4, with 200 mM NaCl at 4°C.

of the aggregates of Δ151–158 Ure2 to the well-formed fibrillar structures typically observed for WT Ure2 (Fig. 5d) or indeed for the mutant Δ15–42 Ure2 (Jiang *et al.*, 2004), although binding to ThT is lost in the Δ15–42 Ure2 mutants (Fig. 4) due to deletion of the hydrophobic region 15–42 (Jiang *et al.*, 2004).

Δ151–158 Ure2 formed fibrils with greater elongation and breakage rate constants than WT Ure2

The successful propagation of a prion depends on the capacity of the soluble protein to convert to the fibrillar form to promote the multiplication of prion seeds and their transmission to other cells. Not only the elongation rate but also the breakage rate of amyloid fibrils has been demonstrated to be crucial for prion propagation (Collins *et al.*, 2004; Smith *et al.*, 2006; Tanaka *et al.*, 2006). Consequently characterizing the kinetic parameters governing fibril growth proves to be very important. Here, we measured the kinetics of fibril growth of WT Ure2 and Δ151–158 Ure2 in order to shed light on the kinetics of prion assembly from a quantitative point of view. We analyzed fibril growth measurements using a master equation (Knowles *et al.*, 2009) which includes the three key processes governing amyloid growth: nucleation, elongation and breakage. This picture includes three kinetic constants: the nucleation rate constant (k_n), the elongation rate constant (k_+) and the breakage rate constant (k_-). In the presence of preformed seed fibrils, the lag time of the fibril formation can be circumvented, which is consistent with a nucleation mechanism (Taylor *et al.*, 1999; Thual *et al.*, 1999; Schlumpberger *et al.*, 2000), and soluble Ure2 will polymerize onto the end of existing seeds with a rate of k_+, which is generally found to be faster than spontaneous formation of nuclei (Jarrett and Lansbury, 1993); indeed under the conditions used here, even in the presence of a small concentration of preformed fibrils, the polymerization reaction reached completion before measurable polymerization took place in samples lacking seed fibrils (Fig. 6). Therefore, in the presence of seed fibrils, the contribution to the overall reaction of spontaneous nucleation events can be neglected and only two constants (k_+, k_-) characteristic of the system are left.

In order to ensure that the number of WT Ure2 and Δ151–158 Ure2 fibril ends in different batches of seed are identical, we performed cross-seeding experiments such that the same WT Ure2 or Δ151–158 Ure2 seed stock solution was used in a given experiment to seed solutions of both proteins. It was found that WT Ure2 and Δ151–158 Ure2 could be seeded by each other (Fig. 6) and the kinetic parameters of fibril formation were obtained by fitting the data globally to an explicit analytical solution to the master equation of fibrillar growth (Knowles *et al.*, 2009). Then the ratios $r_\pm$ of the rate constants $k_\pm$ for growth reactions of WT Ure2 or Δ151–158 Ure2 were calculated from the fitted kinetic parameters (see Materials and Methods section) and summarized in Table II. Regardless of which protein was used as the seed, the ratios of both the elongation and the breakage rate constants were significantly >1, indicating that fibrils grown from Δ151–158 Ure2 possess a higher elongation rate and breakage rate than those grown from WT Ure2, meaning that the Δ151–158 Ure2 fibrils grew and fragmented faster than those of WT. The larger elongation and breakage rates of Δ151–158 Ure2 may contribute to its enhanced prion inducing ability *in vivo*. The nature of the protein seed was observed to have up to a 2-fold effect on the ratios of elongation and breakage rates (Table II), suggesting that the elongation and breakage rates of fibrils formed by WT Ure2 or Δ151–158 Ure2 are dependent on both the nature of the seed and that of the soluble protein; this was also found for breakage rates of homologues of Ure2 from different species of yeast (Y.Q.W., A. Buell, X.Y. Wang, M. Welland, C.M. Dobson, T.P.J. Knowles and S.P., submitted for publication).

Deletion of residues 151–158 disrupts the inhibitory effect of Ydj1 on amyloid-like aggregation of Ure2

Molecular chaperones play a crucial role in the cell by safeguarding proteins from misfolding and aggregation, particularly under conditions of stress, such as heat shock or disease (Walter and Buchner, 2002; Young *et al.*, 2004). Like other heat-shock proteins (Jones and Tuite, 2005), Hsp40 members have been found to play a role in yeast prion propagation. Ydj1 from *S. cerevisiae* is a molecular chaperone of the type I Hsp40 family. Overexpression of Ydj1 results in the loss of the [*URE3*] prion (Moriyama *et al.*, 2000) and also cures certain variants of another yeast prion [PIN^+]/[RNQ^+] (Bradley *et al.*, 2002). Ydj1 has a specific effect on [*URE3*] that is not replicated by overexpression of other J-domain-containing proteins (Lian *et al.*, 2007; Higurashi *et al.*, 2008), although overexpression of an isolated J-domain is sufficient to cause curing of [*URE3*] and a point mutation (H34Q) that disrupts functional interaction with Hsp70 also disrupts the curing effect on [*URE3*], suggesting that the effect of Ydj1 overexpression *in vivo* is mediated by Hsp70 (Higurashi *et al.*, 2008). Our previous studies have shown that *in vitro* Ydj1 inhibits Ure2 fibril formation by binding to the native state of Ure2, prior to the onset of oligomerization (Lian *et al.*, 2007). To ascertain whether the deletion of residues 151–158 affects the interactions between Ure2 and Ydj1, we examined the effect of Ydj1 on the fibril formation of Δ151–158 Ure2. (In order to facilitate comparison, we used a 2-fold higher concentration of WT Ure2 than

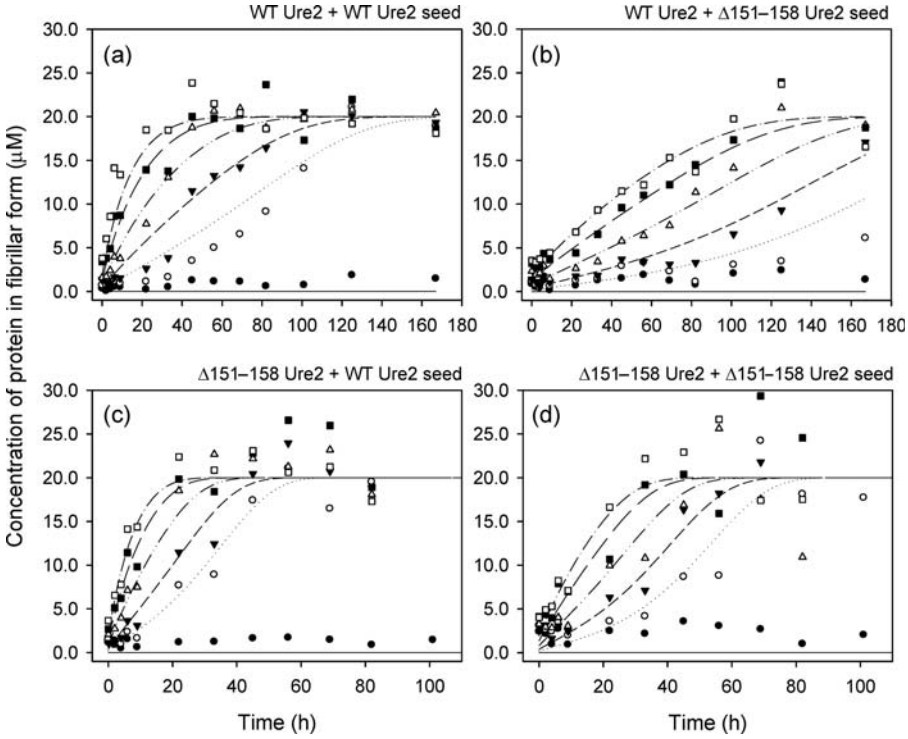

Fig. 6. Time-courses of fibril formation in solution seeding experiments. 20 μM WT Ure2 (**a** and **b**) or Δ151–158 Ure2 (**c** and **d**) were incubated with a series of concentrations of WT Ure2 seed (a and c) or Δ151–158 Ure2 seed (b and d): 0% seed (closed circle), 1% seed (open triangle), 2% seed (closed inverted triangle), 4% seed (open inverted triangle), 7% seed (closed square) and 10% seed (open square), in 50 mM Tris–HCl, pH 8.4, 200 mM NaCl. The data were fitted globally to obtain the rate constants for elongation and breakage, as described in the Materials and Methods section.

Table II. Ratios of elongation and breakage rate constants of fibrils formed from Δ151–158 Ure2 and WT Ure2 in solution cross-seeding experiments

Seed	Ratio (Δ151–158 : WT)	Value
WT	r_+	1.8 ± 0.1
Δ151–158	r_+	3.5 ± 0.4
WT	r_-	5.1 ± 0.9
Δ151–158	r_-	3.2 ± 0.7
Δ151–158 / WT	η_+	1.9 ± 0.3
Δ151–158 / WT	η_-	0.6 ± 0.2

The values shown represent the mean and the standard error derived from the global fit of the data (see Materials and Methods section), where $r_+ = k_+^{\Delta 151-158}/k_+^{WT}$ and $r_- = k_-^{\Delta 151-158}/k_-^{WT}$, with the superscript denoting the protein in solution; and $\eta_+ = r_+^{\Delta 151-158}/r_+^{WT}$ and $\eta_- = r_-^{\Delta 151-158}/r_-^{WT}$, with the superscript denoting the protein in the seed [see equations (12)–(16)]. A value of r_+ or $r_- > 1$ means that the elongation or breakage rate, respectively, for the mutant protein is greater than for WT; a value of η_+ or η_- that deviates from unity indicates that the nature of the protein seed influences the elongation or breakage rate, respectively.

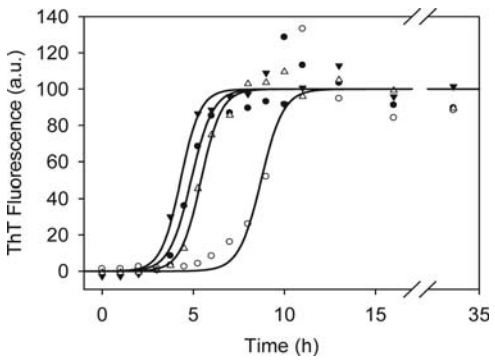

Fig. 7. The effect of Ydj1 on the fibril formation of WT Ure2 and Δ151–158 Ure2. 20 μM WT Ure2 (closed and open circles) and 10 μM Δ151–158 Ure2 (closed inverted triangle, open triangle) were incubated alone (filled symbols) or with an equimolar concentration of Ydj1 (open symbols) in 50 mM NaH_2PO_4-Na_2HPO_4, pH 7.5, 150 mM KCl, 5 mM $MgCl_2$, 1 mM DTT, with agitation at 25°C. The concentration of WT protein was twice that of Δ151–158 Ure2, and the ThT values were normalized, for ease of comparison.

Δ151–158 Ure2, so that the rates of fibril formation for the two proteins in the absence of chaperone were similar, and incubated each protein with or without an equimolar concentration of Ydj1.) As found previously (Lian *et al.*, 2007), the presence of Ydj1 significantly increases the lag time of the fibril formation of WT Ure2 (Fig. 7). However, in comparison, the inhibitory effect of Ydj1 on the aggregation of Δ151–158 Ure2 was significantly reduced (Fig. 7). These results suggest that the deletion of residues 151–158 alters the interaction of Ydj1 with the native state of Ure2 and thus decreases the ability of Ydj1 to inhibit the fibril formation of Ure2 *in vitro*. While the *in vivo* significance of this result has yet to be ascertained, it does imply that deletion of residues 151–158 may affect the interaction of Ure2 with chaperones and other partner proteins.

Implications for the mechanism of prion formation

Recent studies have shown that mutations affecting the prion properties of Ure2 are not restricted to the N-terminal PrD. Deletion of residues 221–227, 151–158 or 348–354 was found to decrease or increase the *in vivo* prion-inducing propensity of Ure2 when the mutant is overexpressed in a WT background, with Δ151–158 producing a 100-fold increase in the rate of induction compared to overexpression of WT

itself (Maddelein and Wickner, 1999). Similarly, a series of point mutations that increase the rate of prion induction have been identified (Fernandez-Bellot *et al.*, 2000): a pair of mutations in the N-terminus (S10L and R17C) combined with a single mutation in the C-terminus (K127E) results in a 500-fold increase in the prion induction rate of Ure2; and a mutation pair (S10L/V271E) is 10 times more efficient than WT at inducing the [*URE3*] prion (Fernandez-Bellot *et al.*, 2000). The results of these mutagenesis studies imply not only the involvement of the C-terminal region in the mechanism of prion induction, but also that there is interplay between the N-terminal and C-terminal regions of the protein. In this study, we investigated the folding and fibril formation properties *in vitro* of Δ151–158 Ure2, which shows enhanced rates of prion induction *in vivo*, in order to obtain insight into the molecular mechanism of prion induction and propagation of Ure2.

Various models have been proposed to describe the mechanism of amyloid or prion formation (Harper and Lansbury, 1997; Kelly, 2000). In general, amyloidogenic proteins show a sigmoidal time-course for fibril formation and the lag time can be reduced or circumvented by the addition of preformed fibril seeds indicating that the process involves a nucleation step. A common feature of the various models is the involvement of partially folded (or misfolded) intermediate states, implying that the mechanism of amyloid or prion formation is related to the pathway by which the protein folds (or misfolds). Therefore, characterization of the folding behavior of prion proteins is an important step in elucidating the mechanism of prion formation. The equilibrium denaturation of Ure2 shows that Ure2 folds via a dimeric intermediate (Zhu *et al.*, 2003b) and our previous studies on the conditions affecting the folding and amyloid formation of Ure2 have suggested that the formation of the Ure2 amyloid precursor involves at least partial unfolding of the native dimer (Zhu *et al.*, 2003b). Kinetic experiments detect population of two distinct intermediates during refolding of Ure2: a 'burst phase' intermediate formed within the dead-time of stopped-flow mixing and a dimeric intermediate (Galani *et al.*, 2002). The dimeric intermediate (I_2) is known to be on-pathway, and the burst phase intermediate is known to be monomeric (Perrett *et al.*, 1999; Galani *et al.*, 2002). The relationship of the monomeric intermediate to the folding pathway is not certain, but conditions that favor population of the monomeric intermediate also favor aggregation (Perrett *et al.*, 1999; Galani *et al.*, 2002). Here, we examined the effect of residues 151–158 on the folding properties of Ure2 *in vitro* and found that, similar to WT Ure2, Δ151–158 Ure2 shows a three-state denaturation process via a dimeric intermediate (Fig. 3). However, compared with WT Ure2, the deletion of residues 151–158 did not cause any significant change in thermodynamic stability (Table I). Further deletions of parts of the PrD showed no effect on the equilibrium unfolding of Δ151–158 Ure2, as was found previously for WT (Perrett *et al.*, 1999; Zhu *et al.*, 2003b). Thus, it is unfortunate that in this case, nothing regarding the role of protein stability or the relative population of the various folding intermediates can be deduced. However, the results do indicate that in the case of Δ151–158, its enhanced propensity to induce a prion state *in vivo* is not due to an alteration in propensity to unfold or populate folding intermediates.

Consistent with its enhanced prion-inducing ability *in vivo*, the deletion of residues 151–158 increased the fibril formation of Ure2 *in vitro* demonstrated by a significantly shortened lag time in the time-course of fibril formation monitored by the ThT assay (Fig. 4). Δ151–158 Ure2 tended to form granular aggregates rather than the typical amyloid-like fibrils formed by WT Ure2 (Fig. 5). These spherical particles appear to be at least partially ordered because they could also bind to the amyloid-specific dye ThT and emit fluorescence. Importantly, the aggregates formed from WT Ure2 and Δ151–158 Ure2 could be seeded by each other (Fig. 6), implying that they possess similar basic structures. Furthermore, this provides a mechanistic explanation for the observation that overexpression of Δ151–158 Ure2 induces the [*URE3*] prion state in a WT background.

As for WT Ure2 (Jiang *et al.*, 2004), further deletions in the PrD decreased the fibril formation of Δ151–158 Ure2. The mechanism by which deletion of the normal random sequence region 15–42 restored the amyloid morphology of Δ151–158 Ure2 (Fig. 5) is not yet understood and is worthy of further investigation. In addition to the faster nucleation rate of Δ151–158 Ure2 implied by the shorter lag time observed in un-seeded ThT assay curves (Fig. 4), cross-seeding experiments between WT Ure2 and Δ151–158 Ure2 showed greater elongation and breakage rate constants for the fibrils formed from Δ151–158 Ure2 compared to those formed from WT Ure2 (Fig. 6 and Table II). These results potentially explain the mechanism by which the deletion of the 151–158 region increases the rate of prion induction by Ure2 overexpression *in vivo,* that is, by increasing both the rate of nucleation and the ease of propagation of prion seeds. Whether the Δ151–158 Ure2 protein itself can maintain the [*URE3*] prion state, or whether it merely seeds the WT protein to form [*URE3*], will require further *in vivo* experiments to ascertain.

Acknowledgements

We thank the staff of the Institute of Biophysics Electron Microscopy Centre for assistance with electron microscopy experiments.

Funding

This work was supported by grants from the National Natural Science Foundation of China (30620130109, 30870482, 31070656, 31000342), the Chinese Ministry of Science and Technology (2006CB500703, 2006CB910903) and the Chinese Academy of Sciences (KSCX2-YW-R-119, KSCX2-YW-R-256).

References

Bai,M., Zhou,J.M. and Perrett,S. (2004) *J. Biol. Chem.*, **279**, 50025–50030.

Baxa,U., Speransky,V., Steven,A.C. and Wickner,R.B. (2002) *Proc. Natl Acad. Sci. USA*, **99**, 5253–5260.

Baxa,U., Cheng,N., Winkler,D.C., *et al.* (2005) *J. Struct. Biol.*, **150**, 170–179.

Baxa,U., Wickner,R.B., Steven,A.C., Anderson,D.E., Marekov,L.N., Yau,W.M. and Tycko,R. (2007) *Biochemistry*, **46**, 13149–13162.

Bousset,L., Belrhali,H., Janin,J., Melki,R. and Morera,S. (2001a) *Structure*, **9**, 39–46.

Bousset,L., Belrhali,H., Melki,R. and Morera,S. (2001b) *Biochemistry*, **40**, 13564–13573.

Bousset,L., Thomson,N.H., Radford,S.E. and Melki,R. (2002) *EMBO J.*, **21**, 2903–2911.

Bradley,M.E., Edskes,H.K., Hong,J.Y., Wickner,R.B. and Liebman,S.W. (2002) *Proc. Natl Acad. Sci. USA*, **99** (Suppl. 4), 16392–16399.
Collins,S.R., Douglass,A., Vale,R.D. and Weissman,J.S. (2004) *PLoS Biol.*, **2**, e321.
Cooper,T.G. (2002) *FEMS Microbiol. Rev.*, **26**, 223–238.
Coschigano,P.W. and Magasanik,B. (1991) *Mol. Cell Biol.*, **11**, 822–832.
Edskes,H.K. and Wickner,R.B. (2002) *Proc. Natl Acad. Sci. USA*, **99** (Suppl. 4), 16384–16391.
Fernandez-Bellot,E., Guillemet,E. and Cullin,C. (2000) *EMBO J.*, **19**, 3215–3222.
Galani,D., Fersht,A.R. and Perrett,S. (2002) *J. Mol. Biol.*, **315**, 213–227.
Grimsley,J.K., Scholtz,J.M., Pace,C.N. and Wild,J.R. (1997) *Biochemistry*, **36**, 14366–14374.
Harper,J.D. and Lansbury,P.T., Jr. (1997) *Annu. Rev. Biochem.*, **66**, 385–407.
Higurashi,T., Hines,J.K., Sahi,C., Aron,R. and Craig,E.A. (2008) *Proc. Natl Acad. Sci. USA*, **105**, 16596–16601.
Jarrett,J.T. and Lansbury,P.T., Jr (1993) *Cell*, **73**, 1055–1058.
Jiang,Y., Li,H., Zhu,L., Zhou,J.M. and Perrett,S. (2004) *J. Biol. Chem.*, **279**, 3361–3369.
Jones,G.W. and Tuite,M.F. (2005) *Bioessays*, **27**, 823–832.
Kelly,J.W. (2000) *Nat. Struct. Biol.*, **7**, 824–826.
Knowles,T.P., Waudby,C.A., Devlin,G.L., Cohen,S.I., Aguzzi,A., Vendruscolo,M., Terentjev,E.M., Welland,M.E. and Dobson,C.M. (2009) *Science*, **326**, 1533–1537.
LeVine,H., 3rd (1993) *Protein Sci.*, **2**, 404–410.
Lian,H.Y., Jiang,Y., Zhang,H., Jones,G.W. and Perrett,S. (2006) *Biochim. Biophys. Acta*, **1764**, 535–545.
Lian,H.Y., Zhang,H., Zhang,Z.R., Loovers,H.M., Jones,G.W., Rowling,P.J., Itzhaki,L.S., Zhou,J.M. and Perrett,S. (2007) *J. Biol. Chem.*, **282**, 11931–11940.
Maddelein,M.L. and Wickner,R.B. (1999) *Mol. Cell Biol.*, **19**, 4516–4524.
Masison,D.C. and Wickner,R.B. (1995) *Science*, **270**, 93–95.
Moriyama,H., Edskes,H.K. and Wickner,R.B. (2000) *Mol. Cell Biol.*, **20**, 8916–8922.
Perrett,S. and Jones,G.W. (2008) *Curr. Opin. Struct. Biol.*, **18**, 52–59.
Perrett,S., Freeman,S.J., Butler,P.J. and Fersht,A.R. (1999) *J. Mol. Biol.*, **290**, 331–345.
Schlumpberger,M., Wille,H., Baldwin,M.A., Butler,D.A., Herskowitz,I. and Prusiner,S.B. (2000) *Protein Sci.*, **9**, 440–451.
Smith,J.F., Knowles,T.P., Dobson,C.M., Macphee,C.E. and Welland,M.E. (2006) *Proc. Natl Acad. Sci. USA* **103**, 15806.
Tanaka,M., Collins,S.R., Toyama,B.H. and Weissman,J.S. (2006) *Nature*, **442**, 585–589.
Tanford,C. (1968) *Adv. Protein Chem.*, **23**, 121–282.
Taylor,K.L., Cheng,N., Williams,R.W., Steven,A.C. and Wickner,R.B. (1999) *Science*, **283**, 1339–1343.
Thual,C., Komar,A.A., Bousset,L., Fernandez-Bellot,E., Cullin,C. and Melki,R. (1999) *J. Biol. Chem.*, **274**, 13666–13674.
Thual,C., Bousset,L., Komar,A.A., Walter,S., Buchner,J., Cullin,C. and Melki,R. (2001) *Biochemistry*, **40**, 1764–1773.
Umland,T.C., Taylor,K.L., Rhee,S., Wickner,R.B. and Davies,D.R. (2001) *Proc. Natl Acad. Sci. USA*, **98**, 1459–1464.
Walter,S. and Buchner,J. (2002) *Angew. Chem. Int. Ed. Engl.*, **41**, 1098–1113.
Wickner,R.B. (1994) *Science*, **264**, 566–569.
Young,J.C., Agashe,V.R., Siegers,K. and Hartl,F.U. (2004) *Nat. Rev. Mol. Cell Biol.*, **5**, 781–791.
Zhang,Z.R. and Perrett,S. (2009) *J. Biol. Chem.*, **284**, 14058–14067.
Zhang,Z.R., Bai,M., Wang,X.Y., Zhou,J.M. and Perrett,S. (2008) *J. Mol. Biol.*, **384**, 641–651.
Zhou,J.M., Zhu,L., Balny,C. and Perrett,S. (2001) *Biochem. Biophys. Res. Commun.*, **287**, 147–152.
Zhu,L., Kihara,H., Kojima,M., Zhou,J.M. and Perrett,S. (2003a) *Biochem. Biophys. Res. Commun.*, **311**, 525–532.
Zhu,L., Zhang,X.J., Wang,L.Y., Zhou,J.M. and Perrett,S. (2003b) *J. Mol. Biol.*, **328**, 235–254.